Bulletin of the Seismological Society of America, Vol. 101, No. 5, pp. 2029–2044, October 2011, doi: 10.1785/0120110039

An Improved Automatic Scheme for Empirical Baseline Correction of Digital Strong-Motion Records

by Rongjiang Wang, Bernd Schurr, Claus Milkereit, Zhigang Shao, and Mingpei Jin

Abstract Compared with seismic waves, near-field static deformation can provide more robust constraints on earthquake size and slip distribution because it is less sensitive to the rupture process and Earth structure. The static deformation data are now obtained using space-geodetic measurements. For early warning and rapid hazard assessment, such geodetic measurements are less useful because they are usually available only with a time delay of days to weeks or even longer. Recent studies have shown that coseismic static displacements can be estimated from modern seismometer records after an appropriate correction for baseline errors that may be caused by rotational motion, tilt, instrument, and other effects. For this purpose, several empirical baseline correction methods have been proposed. Algorithms, in which an acceleration or other acceleration record derived threshold is used to determine the timing of baseline shift, can be easily implemented. In practice, however, the baseline shift is not necessarily accompanying the strongest ground shaking; methods based on the threshold approach tend to lead to an over- or underestimation of the true baseline shift. Other correction schemes, which can be performed by manual calibration, rely on subjective decisions for the choice of correction parameters. In this paper, an automatic scheme is presented, in which the method used to determine the baseline shift has a stronger physical basis. Case studies on the 1999 Chi-Chi, 2007 Tocopilla, 2008 Wenchuan, and 2010 Maule earthquakes, where the strong-motion data were obtained from different types of accelerometers, show that this automatic scheme is more robust than the previously suggested ones. In all test cases, the coseismic displacements recovered from the strong-motion records agree within 10%–20% with direct GPS measurements or indirect model predictions. In addition, the automatic scheme was also successfully used to correct the strong-motion records of a low-cost sensor obtained from a laboratory test.

Introduction

Since the first strong-motion accelerograms were recorded from the 1933 Long Beach (California) earthquake, numerous accelerometers have been installed around the world, accumulating a huge database of strong-motion records. Several recent large destructive earthquakes, such as the 1999 Chi-Chi and 2008 Wenchuan earthquakes, were observed by a dense network of modern digital accelerometers (Lee *et al.*, 2001; Klinger *et al.*, 2010). The strong-motion data provide seismologists and engineers with valuable insight into the nature of seismic ground shaking close to the earthquake source (Boore and Bommer, 2005). However, as with all other physical measurements, strong-motion records include different sources of noise affecting the information to be retrieved. The most well-known problem is caused by shifts in the reference baseline, which prevent recovery of true ground velocities and displacements through double integration.

Development of methods for the baseline correction and double integration of strong-motion records can be traced back to the 1940s (McComb *et al.*, 1943; Trifunac, 1971). A large part of issues investigated in these early studies is related to the analogue instrumentation, which has fortunately been overcome by modern digital seismographs. However, the causes of baseline shifts are very complex and can be attributed not only to the instrumental effect such as, for example, hysteresis of the transducers (Iwan *et al.*, 1985), but also to the ground rotation and tilting (Boore, 2001; Graizer, 2005, 2006). So far, the baseline adjustment of digital strong-motion records can only be achieved using empirical and approximate approaches (Chao *et al.*, 2009).

In general, the baseline shift only affects the response spectra for periods longer than about 20 s that are of little or no engineering interest (Boore, 2001; Wang, Boore, *et al.*, 2003). For most engineering purposes, therefore, the strong-motion data can be processed using a proper high-pass filter

such as that by Chiu (1997). Notice that high-pass filtering removes not only the baseline errors, but also the low-frequency signal content including permanent displacements. The latter is, however, of particular engineering and seismological interest. In general, the permanent displacement field provides information about the earthquake size and final slip distribution, which is independent of the detailed source rupture process and insensitive to Earth structure. If the fault geometry (strike and dip) is known sufficiently, the slip distribution can be directly inverted from the near-field displacement data. This is the case, for example, for megathrust earthquakes in subduction zones.

Robust slip models for large earthquakes are important ingredients, for example, in tsunami early warning systems. Sobolev *et al.* (2007) showed that varying slip distributions of earthquakes having equal seismic moment might locally produce tsunami run-up heights that differ by a factor of 5 and more. They also demonstrated that it is possible to estimate the slip distribution, and hence predict tsunami run-up heights accurately on the basis of near-field static displacement measurements. In general, ground displacement is most accurately measured by geodetic methods. In the last two decades, space-geodetic methods in particular, that is, the Global Positioning System (GPS) and Interferometric Synthetic Aperture Radar (InSAR), have become widely used and valuable tools to study earthquake sources based on careful analysis of induced surface deformation (see, e.g., Segall, 2010). In the context of early warning, however, surface deformation estimates have to be available near real-time, disqualifying most geodetic methods that usually rely on repeat surveys separated by days to months. Only continuous high-rate GPS may have the potential to serve this need. Accurate GPS real-time processing, however, is not yet well established, and high-rate continuous GPS networks are rare. In contrast, strong-motion sensors recording ground acceleration are almost ubiquitous around the world and in particular in seismically active regions. If it would be possible to recover the static displacement in a robust and automatized manner from strong-motion accelerographs, this could be a valuable input for early warning purposes.

This study focuses on how to recover permanent displacement from the strong-motion data and on whether the results are robust enough to be used for routine earthquake source analysis. We begin with a review of currently proposed methods for the baseline correction and then present an improved automatic scheme refined from previously suggested methods that rely on manual adjustment. To validate our algorithm, we choose a series of test cases, which allow comparison of our results against a benchmark either from direct geodetic measurements or indirect model-based predictions. Altogether the test cases assemble a wide range of earthquakes and instrumentation. The purpose of this study is to provide an automatic baseline correction tool that can be used for (near) real-time recovery of near-field coseismic deformation from a dense strong-motion network. It is not expected that the tool works impeccably for each individual record, but it should be robust enough for the whole network in a statistical sense, so that it can be implemented, for example, in tsunami early warning and rapid earthquake information systems.

Review of Currently Proposed Methods

The baseline shift of an accelerogram can be composed of a preevent baseline shift and an event-induced baseline shift. The latter can be further separated into a transient part during the strong ground shaking and a postevent static or quasi-static part after the strong ground shaking. In an ideal case, that is, without any baseline shift, the accelerogram can be integrated once to velocity and twice to displacement. In that case, the pre- and postevent velocity should be around the zero level, whereas the displacement can be approximated by a ramp function (Wu and Wu, 2007).

Empirical methods aim to estimate the baseline shift based on the abnormal behavior of the uncorrected velocity or displacement history after integration without any assumption about the sources of the baseline shift. The preevent baseline shift can easily be evaluated within a preevent window of the acceleration trace, as shown in Figure 1. Similarly, the postevent baseline shift can be evaluated within a postevent window of the acceleration trace. However, the long lasting coda may influence the accuracy of the evaluation for the latter. For this reason, it is usually determined from the linear drift of the velocitogram obtained by integration of the accelerogram after the correction for the preevent baseline shift. The most difficult task of the baseline shift correction is the determination of the transient baseline shift during the strong ground motion. In principle, any oscillatory transient baseline shift with zero average cannot be corrected using such an empirical approach, because it is inseparable from the translational ground motion signal.

Graizer (1979) suggested a polynomial baseline correction that is determined by least-squares fitting to the strong-motion record without weighting the portion containing major signals. A similar method is applied by Zhu (2003) to broadband seismometer records. In practice, however, the results for coseismic displacements derived by this approach are sensitive to the choice of the polynomial degree and signal window.

Iwan *et al.* (1985) assume that the baseline shift is caused by transducer hysteresis of the measurement system and define an average transient baseline offset during the strongest portion of ground shaking and a remaining permanent baseline offset after the strongest portion of the strong ground shaking. Based on their experiments showing that very little transducer hysteresis occurs for accelerations less than 50 cm/s^2, they propose two options for locating the start and end time (t_1 and t_2 in Fig. 1) of the transient baseline offset. Option one is used if there is known to be a final net displacement, for example, in the case of very-near-fault stations. In this option t_1 and t_2 are selected as the first and last times when the absolute acceleration exceeds the 50 cm/s^2

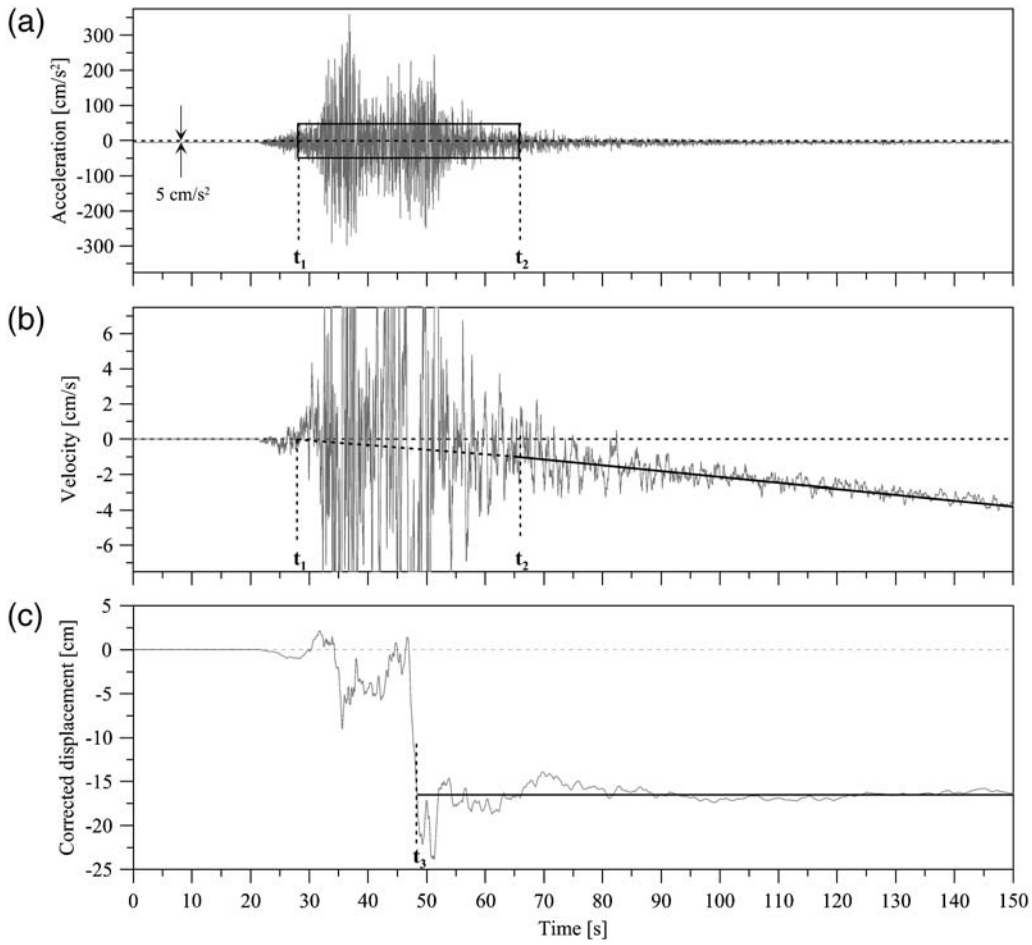

Figure 1. (a) Example of an original accelerometer record showing a preevent baseline offset of 5 cm/s^2. The box marks the strongest portion of ground shaking exceeding a 50 cm/s^2 threshold. (b) Velocitogram obtained by integration of the accelerogram after the correction for the preevent baseline shift. Values exceeding the axis limits are not plotted. The smooth line shows the velocity correction for the event-induced baseline offset using the Iwan *et al.* (1985) approach. See text for explanation. (c) Displacement seismogram obtained by integrating the velocity after the baseline correction. The time at which the ground arrives at the permanent position is denoted by t_3 according to Wu and Wu (2007).

threshold, respectively. Option two is used in the case when it is unknown whether the final net displacement is significant. In this option t_1 is selected as the time of the first significant acceleration pulse, whereas t_2 is determined such that the final net displacement is minimized. Another option was discussed by Boore (2001), in which t_1 is selected at the zero crossing of the postevent linear velocity correction. The whole baseline correction to the velocitogram is expressed in the form of a continuous function

$$v_c(t) = \begin{cases} 0, & t \le t_1 \\ \frac{v_f}{t_2 - t_1}(t - t_1), & t_1 < t < t_2, \\ v_f + a_f(t - t_2), & t \ge t_2 \end{cases} \qquad (1)$$

where the parameters v_f and a_f are determined by least-squares fitting of the function to the postevent velocitogram after time t_2, and the term $\frac{v_f}{t_2 - t_1}$ (denoted as a_m in Iwan *et al.*, 1985) expresses the average of the transient baseline offset in the original accelerogram.

Various case studies (Boore, 2001; Boore *et al.*, 2002; Wang, Boore, *et al.*, 2003, 2007) have shown, however, that the hysteresis of sensors is only one of numerous possible sources of baseline shift. In many cases, the gravity effect due to ground tilting is the dominant source. As the details for the baseline shift differ from case to case, it may not be the best choice to estimate the start time and duration of the transient baseline shift by the described acceleration threshold. In fact, no satisfactory results are obtained using this approach for the 1999 Chi-Chi earthquake. Therefore, Boore (2001) generalized the Iwan *et al.* (1985) method by allowing t_1 and t_2 to be free parameters instead of determining them by static acceleration threshold. He demonstrated that various choices of t_1 and t_2 can lead to a reasonable velocity history but quite different values of the final displacement. Boore's results suggest that the bilinear correction form suggested by Iwan *et al.* (1985) is in general appropriate, but a more reliable criterion for determining t_1 and t_2 has to be applied.

Based on the experience from these previous studies, Wu and Wu (2007) propose an improved baseline correction scheme, in which the bilinear correction form is adopted, but the time parameters t_1 and t_2 are determined in an iterative way so that the corrected displacement history takes the shape of a ramp function. First, the raw data are integrated once to velocity and twice to displacement. Then, t_1 is selected by the time when the ground just starts to move from the zero level, but not earlier than the first exceeding of the 50 cm/s^2 threshold in acceleration, while t_2 is a free parameter varying from t_3 to the end of the record, where t_3 is the time when the ground seems to just arrive at the permanent position. The optimal value of t_2 is found when the corrected displacement history after t_3 has the maximum flatness (Fig. 1). An indicator of the flatness is defined by

$$f = \frac{|r|}{|b| \cdot \sigma}, \tag{2}$$

where b is the slope of the regression line of the corrected displacement history from t_3 to the end of the record, r is the linear correlation coefficient, and σ is the variance. In the last step, the t_1 and t_2 obtained in this way are used to test the baseline correction. If it is necessary, new values of t_1 and t_3 are chosen based on the corrected displacement history, and the procedure for optimizing t_2 is repeated. Wu and Wu (2007) applied their baseline correction approach to all of the strong-motion data of the 1999 Chi-Chi, 2003 Chengkung, and 2006 Taitung earthquakes recorded in the near source region and obtained coseismic displacements consistent with GPS measurements.

The Wu and Wu (2007) approach for determining the time of the baseline shift is physically more reasonable than that by Iwan *et al.* (1985), but it still uses a subjective assessment of the displacement result as the criterion so that an implementation of it for automatic data processing is difficult. Chao *et al.* (2009) simplify the iterative procedure for selecting t_1 and t_3 by two threshold ratios of accumulative acceleration energy. With the optimized threshold values of 25% and 65% for t_1 and t_3, respectively, Chao *et al.* (2009) can reproduce Wu and Wu's (2007) results for most of the relatively large coseismic displacements in the near-fault locations of the 1999 M_w 7.6 Chi-Chi, the 2003 M_w 6.8 Chengkung, and the 2006 M_w 6.1 Taitung earthquakes. However, for locations that are not in the immediate vicinity of the earthquake fault but still show large ground shaking, the automatic scheme of Chao *et al.* (2009) often leads to significant overestimates of the coseismic displacement, compared with Wu and Wu's (2007) manually estimated results. This artifact also appears in the test cases represented later in the present study.

In fact, the automatic scheme by Chao *et al.* (2009) works in a way similar to option two by Iwan *et al.* (1985). In both approaches, t_1 is fixed via threshold and t_2 is optimized. Once a threshold of either acceleration or acceleration energy is used to determine the timing of baseline shift, a common disadvantage appears: it may be able to cover most normal cases, but not all individual special cases, as the baseline shift is related mostly, but not necessarily, to the strongest ground shaking. In this study, we suggest an improved automatic scheme in which the baseline correction is determined by the long-time behavior of the uncorrected

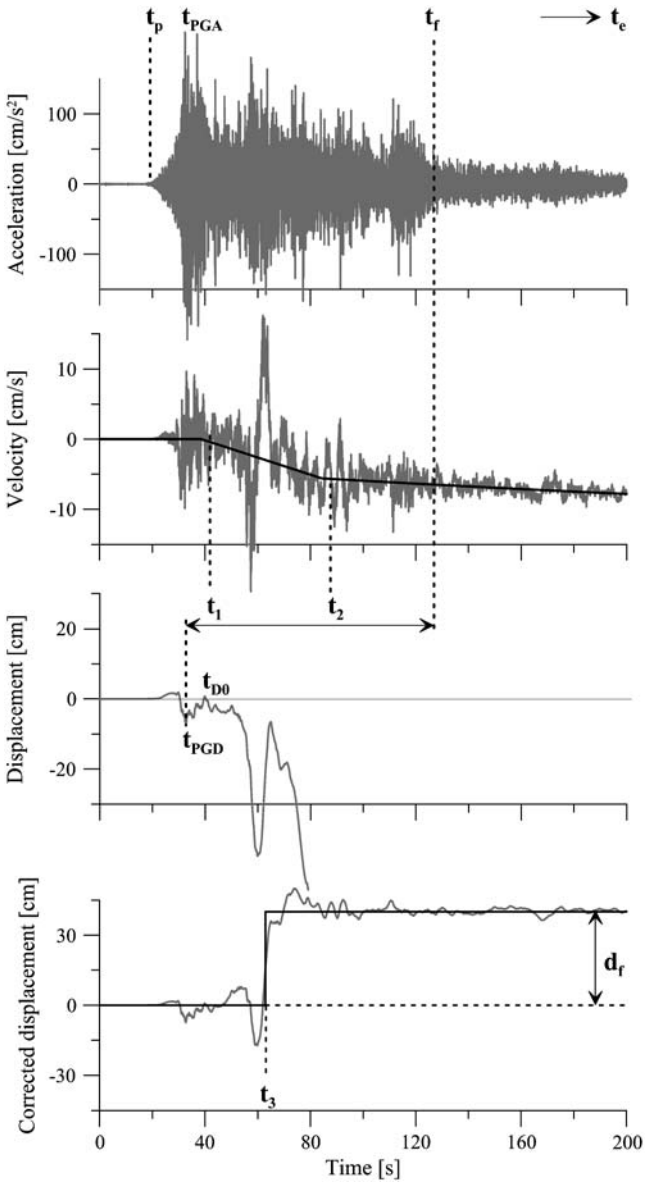

Figure 2. From top to bottom: the east–west component of accelerogram recorded at a station near the southwest fault edge of the 2008 M_w 7.9 Wenchuan earthquake, the velocity and displacement seismograms integrated from the raw data, and the corrected displacement history derived from the strong-motion record using the automatic baseline correction approach developed in this study. The straight line segments on the velocity seismogram show the bilinear baseline correction. t_p, t_{PGA}, t_f, t_e, t_{D0} and t_{PGD} are time parameters used in the automatic baseline correction scheme presented in this study. t_1 and t_2 are the times of the transient and permanent baseline shift, respectively, determined using a grid search approach. The parameters t_3 and d_f defines the step function that best fits the corrected displacement history.

velocity and displacement seismograms, a similar principle as was once used manually by Boore (2001) and Wu and Wu (2007).

An Improved Automatic Baseline Correction Scheme

The baseline shift in an accelerometer record is normally several orders of magnitude smaller than the peak ground acceleration (PGA). In the example shown in Figure 2, the baseline shift is about 0.02 cm/s^2, compared with the PGA of 222 cm/s^2. So it is almost invisible in the raw data, but its effect is clearly shown in the velocity and even more in the displacement history after double integration. Therefore, the beginning of the baseline shift should be traced from the drift of the uncorrected velocity, or even better, from the drift of the uncorrected displacement.

To better illustrate our automatic baseline correction scheme, we first introduce the following characteristic times (all are shown in Fig. 2): t_p = the first arrival of the signal, t_{PGA} = the time of peak ground acceleration during the whole record period, t_{D0} = the time of the last zero crossing of the uncorrected displacement, t_{PGD} = the time of peak ground displacement before time t_{D0}, t_f = the roughly estimated end of the strong ground shaking, and t_e = the end of the record.

As done by Boore (2001), we allow the times marking the beginning of the transient and permanent baseline shift, t_1 and t_2, to be two free parameters. The first issue is how to select a reasonable range of variation for t_1 and t_2. From the long-time behavior of the uncorrected displacement seismogram, it can be assumed that the major signal before t_{D0} is not yet, or at least, not yet significantly affected by the baseline shift. Therefore, we can make a reasonable assumption that the transient baseline shift cannot begin earlier than the time of peak ground displacement before the last zero crossing of the uncorrected displacement, that is, t_{PGD}. The permanent baseline shift should have been established at latest at the end of the strong ground shaking period, denoted by t_f, which we roughly estimate by the time when, for example, 90% of the accumulative acceleration energy has arrived, but not earlier than t_{D0} and t_{PGA}. In summary, we can define a reasonable variation range of t_1 and t_2 as follows,

$$\begin{cases} t_{\mathrm{PGD}} \le t_1 < t_2 \\ \max(t_{D0}, t_{\mathrm{PGA}}) \le t_2 \le t_k \end{cases} . \tag{3}$$

The second issue is what criterion should be used to optimize t_1 and t_2. Wu and Wu (2007) suggest that a near-field displacement history takes the shape of a ramp function with a finite rise time. Based on our experience, however, if this is used for the automatic optimization, it may easily result in an overestimated final displacement with too long of a rise time. In fact, the static displacement is attributed to the near-field terms of seismic waves whose amplitude should theoretically decrease with distance by $1/r^2$ and $1/r^3$ (compared with the geometrical spreading for body and surface waves that decrease with $1/r$ and $1/\sqrt{r}$, respectively). Thus, the rise time of displacement should be comparable with the rupture duration of the nearby fault segment, which is usually only a small fraction of the whole earthquake rupture duration.

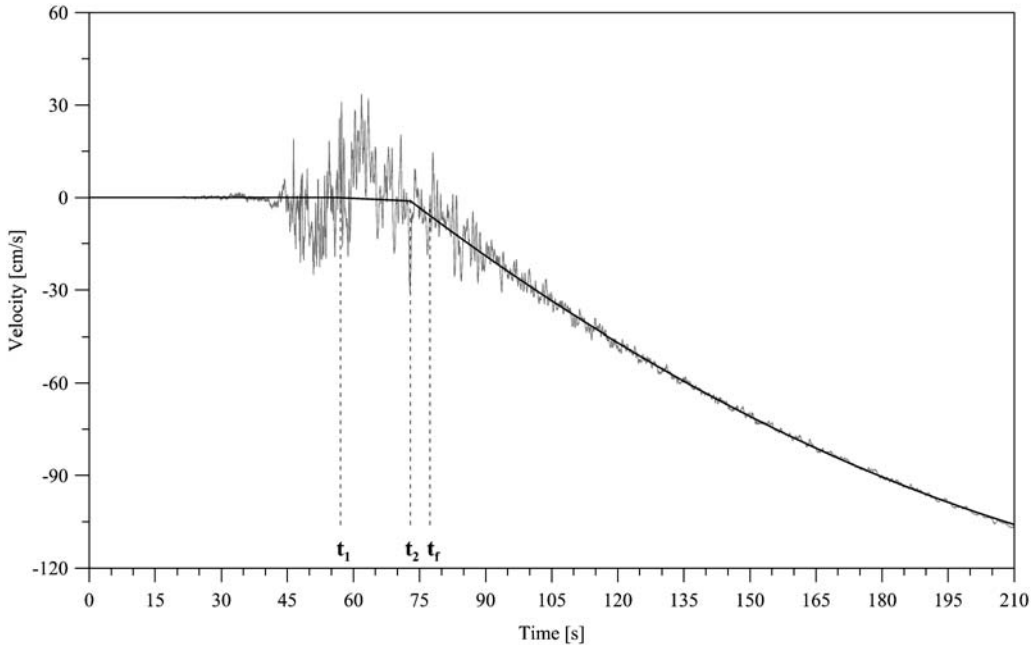

Figure 3. Example of velocitogram integrated from an accelerometer record at station 51JYC (31.96° N, 104.98° E) from the 2008 Wenchuan earthquake with inconstant baseline shift. The smooth line shows the nonlinear trend correction on velocity determined using the automatic scheme presented in this study.

In our approach, we therefore optimize t_1 and t_2 via a grid search approach so that the corrected displacement history best fits a step function, as shown in Figure 2.

The third issue to be solved is which data portion should be used to determine the postevent baseline shift. In previous studies, the parameters v_f and a_f in equation (1) are determined by least-squares fitting of a correction line to the velocity drift between t_2 and the record end t_e. A problem in this approach is that the two parameters describing the postevent drift are sensitive to the location of t_2 when t_2 falls in the major signal window of velocity. To avoid this problem, we use a quadratic function to fit the displacement history from t_f to t_e and then differentiate it to obtain the velocity drift valid from t_2 to t_e. This treatment minimizes the dependence of v_f and a_f on the selection of t_2 and therefore avoids improper correction of the postevent baseline shift.

The fourth and last issue, which has not been discussed so far, is how to account for the effect of the record length on the postevent baseline correction. In practice, slow variations in the postevent baseline shift have been observed. Boore (2001) mentioned that in some records from California earthquakes, he has found subsequent changes in acceleration baseline leading to a nonlinear trend in velocity. We have found similar phenomena in records from the 2008 Wenchuan earthquake. Figure 3 shows an example for a quadratic velocity trend observed at the station 51JYC (31.96° N, 104.98° E). In our approach, the data length is truncated only if it includes a postevent record that is too long (e.g., longer than 4 times the signal window). In the case that the length of the postevent record $(t_e - t_f)$ is comparable with the length of the signal window $(t_f - t_p)$, a quadratic function is used to fit the displacement trend. For a longer postevent window, we check whether a cubic function fits the displacement trend substantially better than a quadratic function, that is, the cubic function will be chosen only if it can at least halve the variance of fitting errors in comparison with the quadratic function.

In summary, our automatic baseline correction is realized by the following procedure:

1. Estimate the first arrival of signal t_p by a threshold approach (e.g., when it exceeds five times the noise level); determine the preevent baseline offset using, for example, 10–20 s preevent window before t_p; and remove the offset from the whole record.
2. Determine t_{PGA} and t_f where t_f is selected by a threshold ratio of accumulative acceleration energy (e.g., 90%). If necessary, cut the postevent record at t_e so that $t_e \le t_p + 4(t_f - t_p)$.
3. Integrate the acceleration to velocity and displacement, and determine t_{D0} and t_{PGD}, as described in the previous steps.
4. Determine a quadratic or, if necessary, a cubic function that best fits the displacement history between t_f and t_e, and obtain the postevent correction parameters v_f and a_f from the derivative of the quadratic or cubic function.
5. Examine all candidate baseline corrections by screening $t_2 \in (\max(t_{\mathrm{PGA}}, t_{D0}), t_f)$ and $t_1 \in (t_{\mathrm{PGD}}, t_2)$, and fit each corrected displacement by a step function $d_f H(t - t_3)$ via a nonlinear regression.

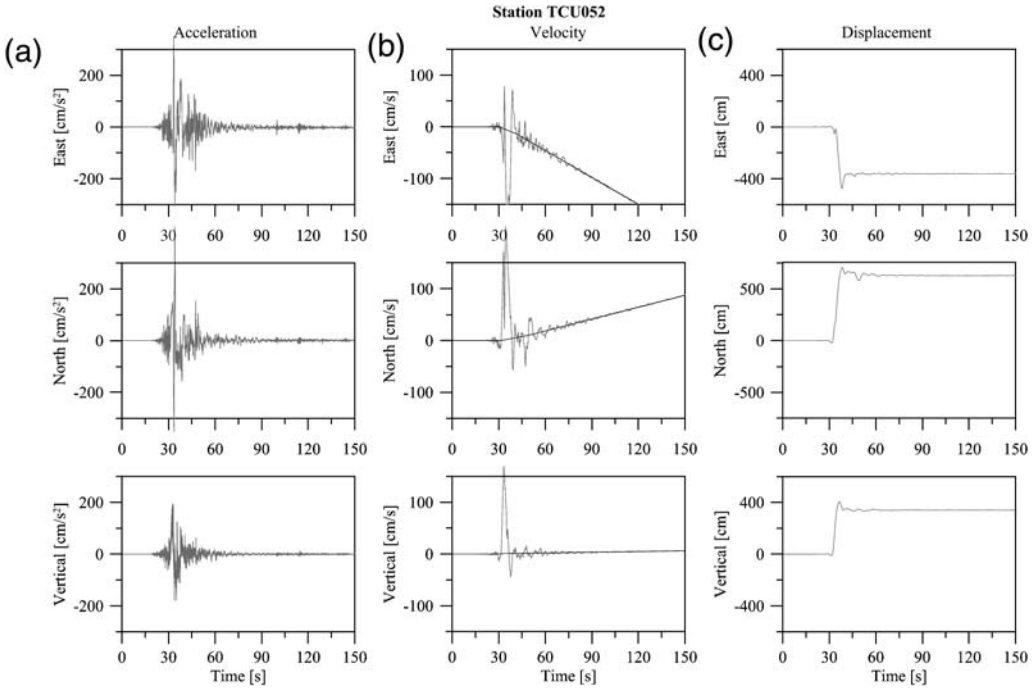

Figure 4. (a) Three components of strong-motion records at station TCU052. (b) Velocity seismograms integrated from the strong-motion records and the trend correction (smooth lines) determined in this study. (c) Displacement seismograms integrated from the corrected velocity seismograms.

6. Select the optimal t_1 and t_2 so that the corrected displacement history best fits a step function, and make the final baseline correction.
7. Determine a ramp function that best fits the finally corrected displacement, and obtain the coseismic displacement from the postevent plateau of the ramp function.

Once the few thresholds are set, the seven steps outlined here require no interference by the user. In the following sections we apply the automatic baseline correction scheme in this way to the strong-motion records from several recent major earthquakes and compare the derived coseismic displacements directly with GPS measurements or indirectly with model-based predictions. Additionally, we validate our method using test data of a low-cost accelerometer with known displacements created in the lab.

The 1999 M_w 7.6 Chi-Chi (Taiwan) Earthquake

As done by Wu and Wu (2007), we select strong-motion records of 10 stations from the database of the Chi-Chi earthquake (Lee *et al.*, 2001) for validating our automatic baseline correction scheme. For these stations there exist GPS displacement data from nearby stations (max. 3.81 km away).

The largest coseismic displacement is obtained from station TCU052 shown in Figure 4. The results produced by our automatic scheme are −364 cm, 632 cm, and 342 cm for the east, north, and vertical components, respectively. These values are very close to the manually calibrated results obtained by Wu and Wu (2007) and consistent with the GPS measurements 2.7 km away (Fig 5). The same is true for the other nine stations (Fig. 6).

The 2007 M_w 7.8 Tocopilla (Chile) Earthquake

This earthquake occurred on the subduction thrust fault in northern Chile and caused substantial damage in the region. Its slip distribution has been well studied using both seismic waveform and space-geodetic data (e.g., Delouis *et al.*, 2009; Motagh *et al.*, 2010). The event occurred at the southern and down-dip end of a known seismic gap. This area is monitored by the network of the Integrated Plate boundary Observatory Chile (IPOC; Schurr *et al.*, 2009; see Data and Resources), a German, French, and Chilean initiative to study deformation processes throughout the subduction seismic cycle. Typical IPOC sites today are equipped with colocated seismic broadband and strong-motion sensors and high-rate continuous GPS receivers. At the time of the earthquake, however, the network was still in its build-up and only parts of the seismic component and isolated GPS sites were operating (Fig. 7). Two strong-motion instruments were located on top of the rupture plane and another nine at various near to regional distances. With the rupture plane for most parts beneath hyperarid land, an excellent InSAR dataset could be collected and processed

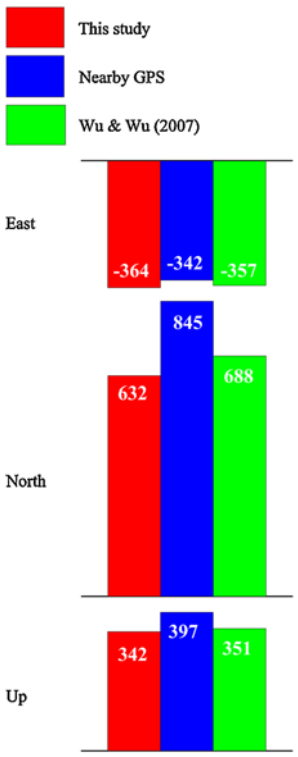

Figure 5. Coseismic displacements in cm derived from strong-motion records at station TCU052 using two different baseline correction methods in comparison with the nearby GPS data. The color version of this figure is available only in the electronic edition.

(Motagh *et al.*, 2010). Altogether this makes an excellent test case because the rupture is well constrained by geodetic data.

We will compare the coseismic displacements derived from the strong-motion records with a surface displacement model based solely on geodetic data. We first derive a slip model of the earthquake by a joint inversion of the three line-of-sight displacement datasets from ENVISAT SAR interferometry (Motagh *et al.*, 2010) and the 3D displacement dataset from the 11 GPS stations (Bejàr *et al.*, 2010). Based on this slip model, we use forward modelling to predict the coseismic deformation at the site of the strong-motion stations.

Figure 8 shows the coseismic displacements obtained by two different automatic baseline correction schemes, compared with the results predicted by the geodetic model. From the comparison we can conclude that the coseismic displacements derived from the strong-motion records are generally consistent with the geodetic results. For stations that are not so close to the earthquake source, the empirical baseline correction is more robust using the improvements developed in this study. There are two exceptions worth noting: the east–west component for station PB2 and the up-down component for station PB8 (Fig. 8). The results for these two components derived from the strong-motion records show the opposite polarity as that predicted by the geodetic slip

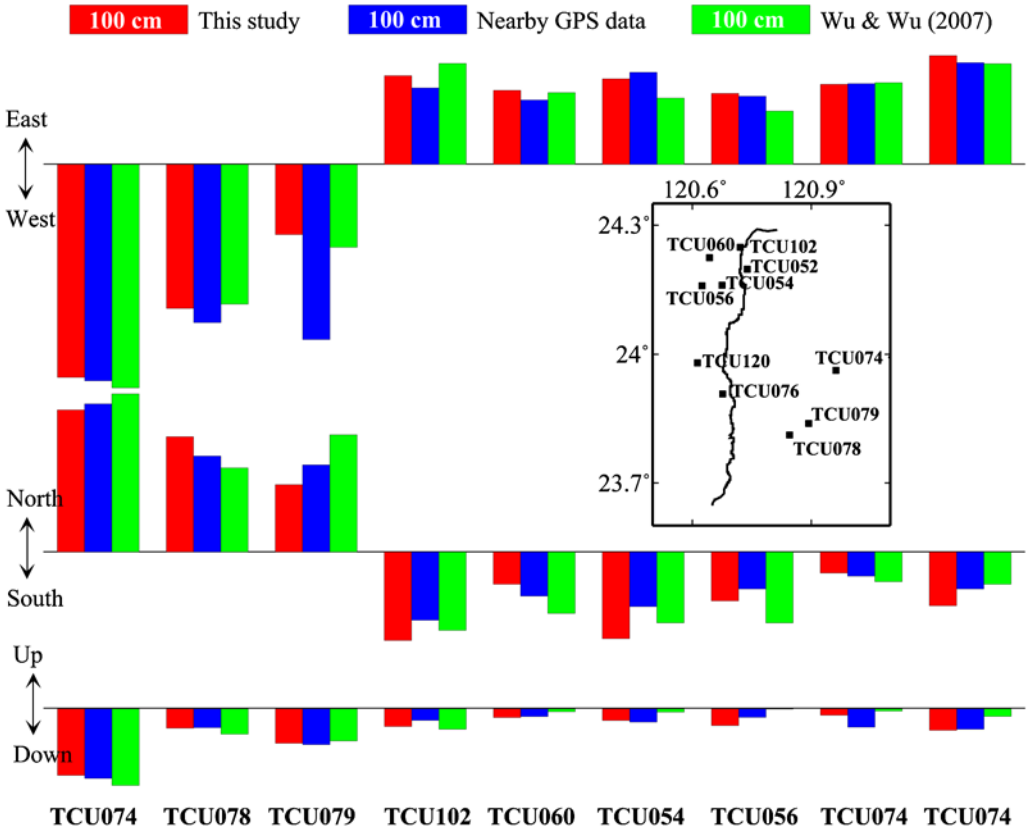

Figure 6. Same as Figure 5, but for nine other stations. The inset map shows the stations and the surface rupture trace of the Chi-Chi earthquake. The color version of this figure is available only in the electronic edition.

model. The problem of the east–west component for station PB2 is probably caused by an unknown instrumental effect in the strong-motion record; there was a large and oscillating baseline drift during the postevent period. Station PB8 is far away from the earthquake source area. The predicted displacement for this station is relatively small and seems to be within the uncertainty of the geodetic model used.

It is interesting to see how well the coseismic displacement data derived from the strong-motion records can be used to constrain the earthquake source parameters. Using a standard least-squares inversion method, we determine the slip distribution from these ground acceleration-based coseismic displacement data alone and compare it with the slip model from the comprehensive geodetic dataset. As suggested by Motagh *et al.* (2010), we use a rectangular fault plane that follows the trace of the trench for 340 km, extending along the dip for 180 km. The dip angle of the plane was assumed to be 20°. The fault plane is represented by 420 discrete dislocation patches, each being ~12 km by 12 km. The surface deformation by each source patch with a unit slip, that is, Green's function, is calculated using the dislocation theory applied to a layered elastic earth model (Wang *et al.*, 2003). As shown in Figure 9, the two slip models are surprisingly well consistent. In particular, the fault size and major slip asperities, which are the source parameters most relevant for a tsunami early warning system (Sobolev *et al.*, 2007), are well constrained by the relatively small dataset based on the near-field strong-motion records.

The 2008 M_w 7.9 Wenchuan (China) Earthquake

The large destructive Wenchuan earthquake occurred on 12 May 2008 at the eastern margin of the Tibetan plateau along the Longmen Shan fault. Excellent field observations were made for this earthquake by a variety of geophysical networks operated by the China Earthquake Administration in cooperation with other Chinese scientific institutions (Zhang *et al.*, 2010). In particular, a large dataset of strong-motion records (Li *et al.*, 2008) and GPS coseismic displacements (Working Group, 2008; Shen *et al.*, 2009; Zhang *et al.*, 2010) are available. More studies on the Wenchuan earthquake can be found in a special issue of the *Bulletin of the Seismological Society of America* (Klinger *et al.*, 2010).

We select all of 62 stations within about 300 km around the fault and apply our automatic baseline correction scheme blindly to the strong-motion records. As expected, large coseismic displacements (≥20 cm) that can be recovered reliably are distributed in the near-field within about 200 km around the fault. As shown in Figure 10, the coseismic displacements derived from the strong-motion records are generally reasonable in the sense of the focal mechanism

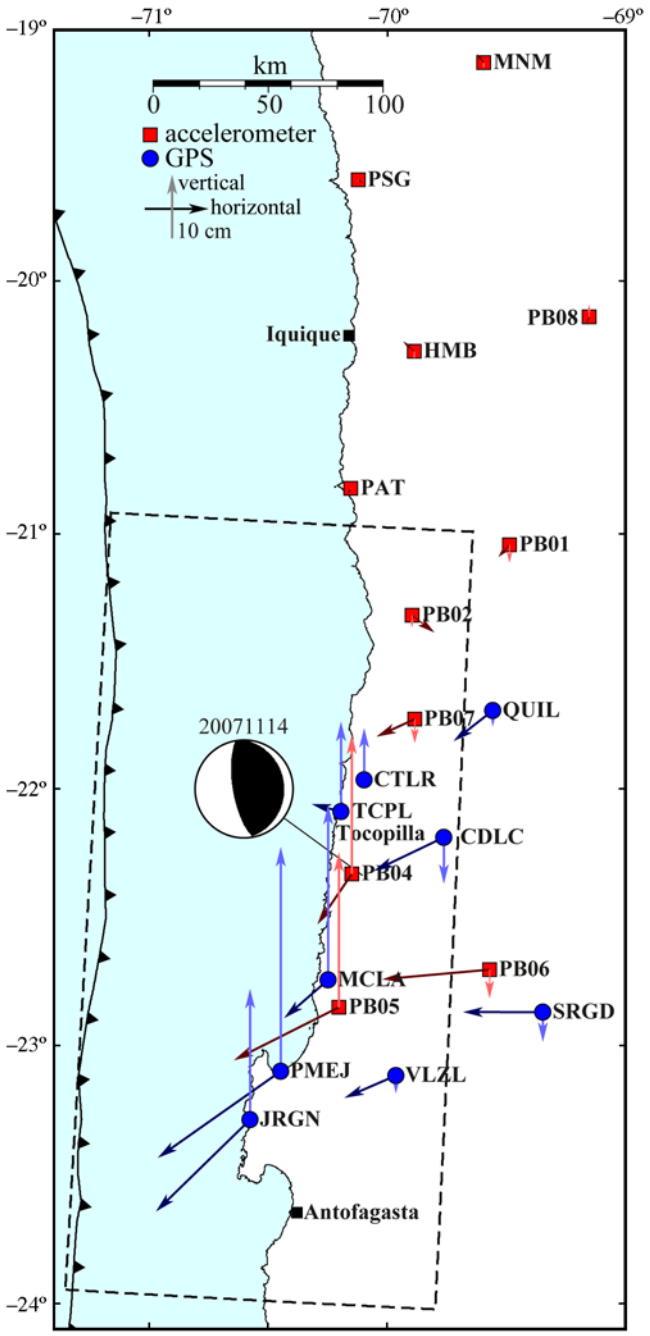

Figure 7. Location map of strong-motion sensors (squares) and GPS sites (circles). Arrows indicate horizontal (dark) and vertical (light) coseismic displacement. For details on the GPS data, see Bejàr-Pizarro *et al.* (2010). The hypocenter is located directly beneath the IPOC station PB04. The dotted rectangle shows the surface projection of the model fault plane. The color version of this figure is available only in the electronic edition.

and consistent with the GPS data, particularly for the horizontal component. In comparison, the results obtained using the Chao *et al.* (2009) method are less robust, particularly for stations showing a nonlinear baseline shift (see Fig. 3).

In the following, we investigate how the strong-motion based coseismic static displacement data can be used to constrain the earthquake source. From previous studies based on near-field geodetic observations, it is known that the Wenchuan earthquake ruptured several segments of the Longmen Shan fault, for a total length of about 300 km, and the fault slip is dominated by thrust movement with a significant right-lateral strike-slip component (Shen *et al.*, 2009; Zhang *et al.*, 2010; Diao *et al.*, 2010; Xu *et al.*, 2010). We use a simplified fault geometry consisting of a single segment that is 300 km long and 40 km wide. The fault trace on the surface is bent slightly to the northwest (Fig. 10). Along dip it takes a listric form with the dip angle linearly decreasing from 60° at the surface to 20° at the bottom in about 25 km depth. The fault plane is represented by an array of 480 discrete source patches, each 5 km by 5 km. Figure 11 shows two slip distributions derived from the GPS and strong-motion based datasets, respectively.

The slip distribution derived from the GPS data consists of at least three large asperities, indicating the multievent characteristic of the earthquake. All of these large asperities can also be identified from the teleseismic waveform that is obtained by stacking 374 broadband records from the USArray in the United States (Yanlu Ma, personal commun., 2009). The slip distribution derived from the acceleration-based coseismic static displacement data clearly resolves the two major asperities. Only the magnitude of the last asperity on the northeast edge is underestimated because of the lack of near-fault strong-motion stations in that area. Moreover, the moment magnitude determined from the two slip models is almost the same, M_w 7.9, which is in a good agreement with the seismological observation.

The 2010 M_w 8.8 Maule (Chile) Earthquake

For this earthquake, the records of an accelerometer and a high-rate (1 Hz) GPS receiver, both colocated at station ROBL (−32.9761° N, −71.0151° E) about 360 km north-northeast of the epicenter (−35.909° N, −72.733° E), are available (Christophe Vigny, personal commun., 2011). We analyze the strong-motion data using our automatic baseline correction scheme blindly, that is, without any adjustment of the parameter settings as used in the previous case studies. The results are shown in Figure 12. All three components of the corrected displacement derived from the accelerogram agree well with the GPS records, validating the robustness of the present baseline correction algorithm. The records agree well even at higher frequencies, because the dominant frequencies in the ground displacement are so low that aliasing does not seem to be an issue for the 1 Hz sampling of the GPS measurements. This is demonstrating the feasibility of using continuous GPS data as long-period seismometers. Figure 12 shows also the static displacement derived from the daily GPS solutions (Christophe Vigny, personal commun., 2011) before and after the earthquake. This should best present the true static displacement. It is interesting to note that the *a posteriori* 1 Hz GPS solution shows an error in postevent static displacement of similar

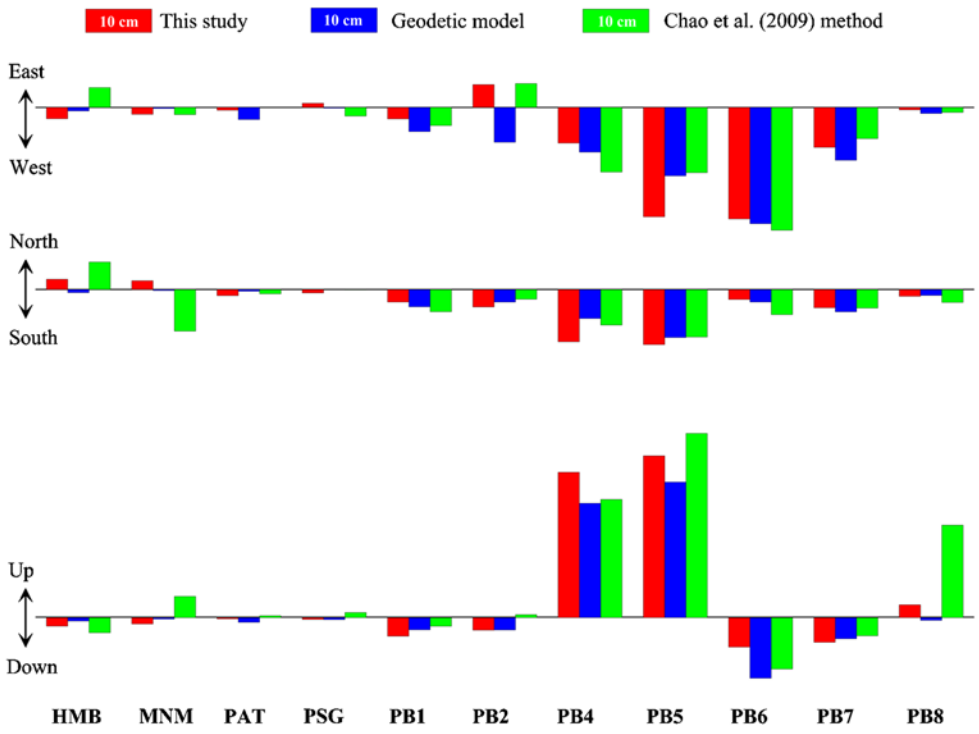

Figure 8. Coseismic displacements derived from the strong-motion records of the 2007 M_w 7.8 Tocopilla earthquake using two different automatic baseline correction schemes, compared with the results predicted using a geodetic model. The color version of this figure is available only in the electronic edition.

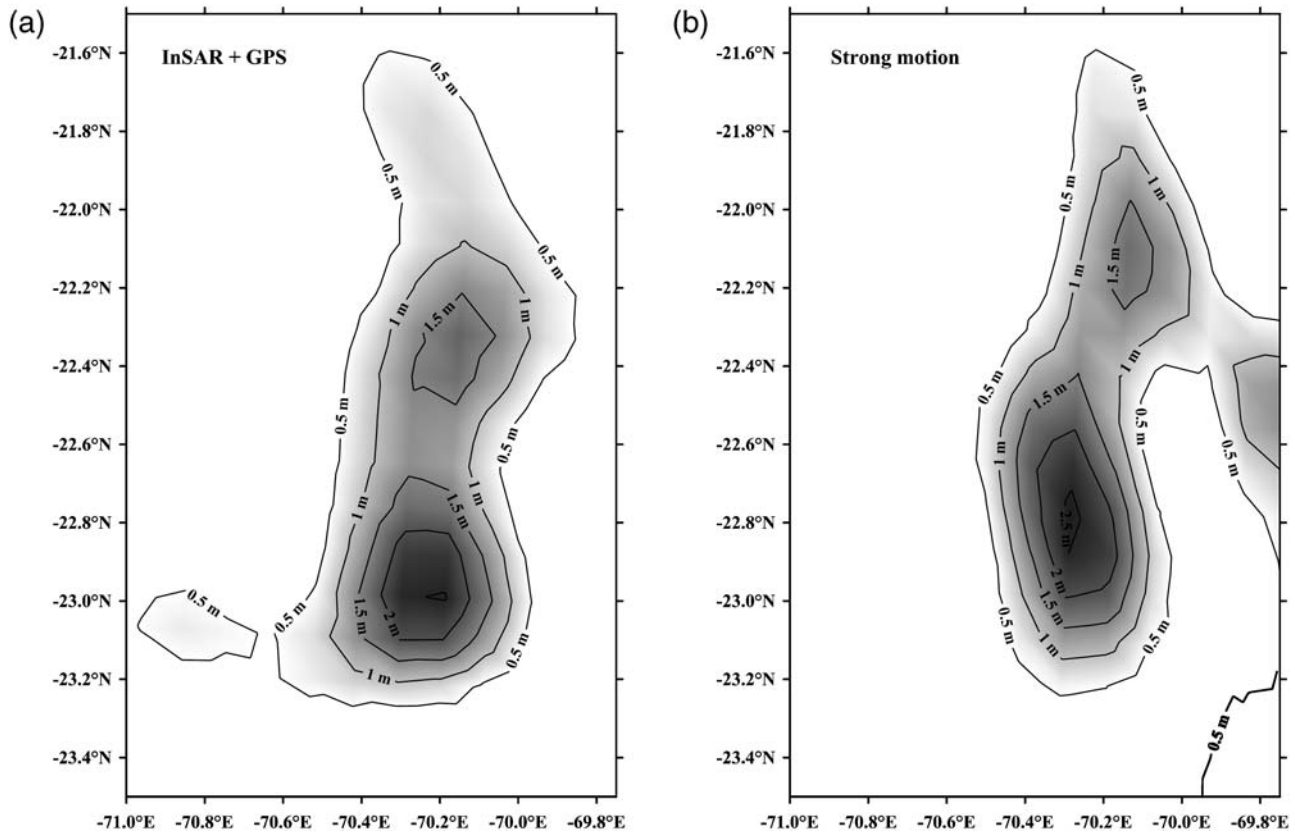

Figure 9. Comparison between the geodetic and seismological source models of the Tocopilla earthquake. (a) Slip distribution based on the InSAR and GPS data. (b) Slip distribution based on the coseismic displacement data derived from the strong-motion records.

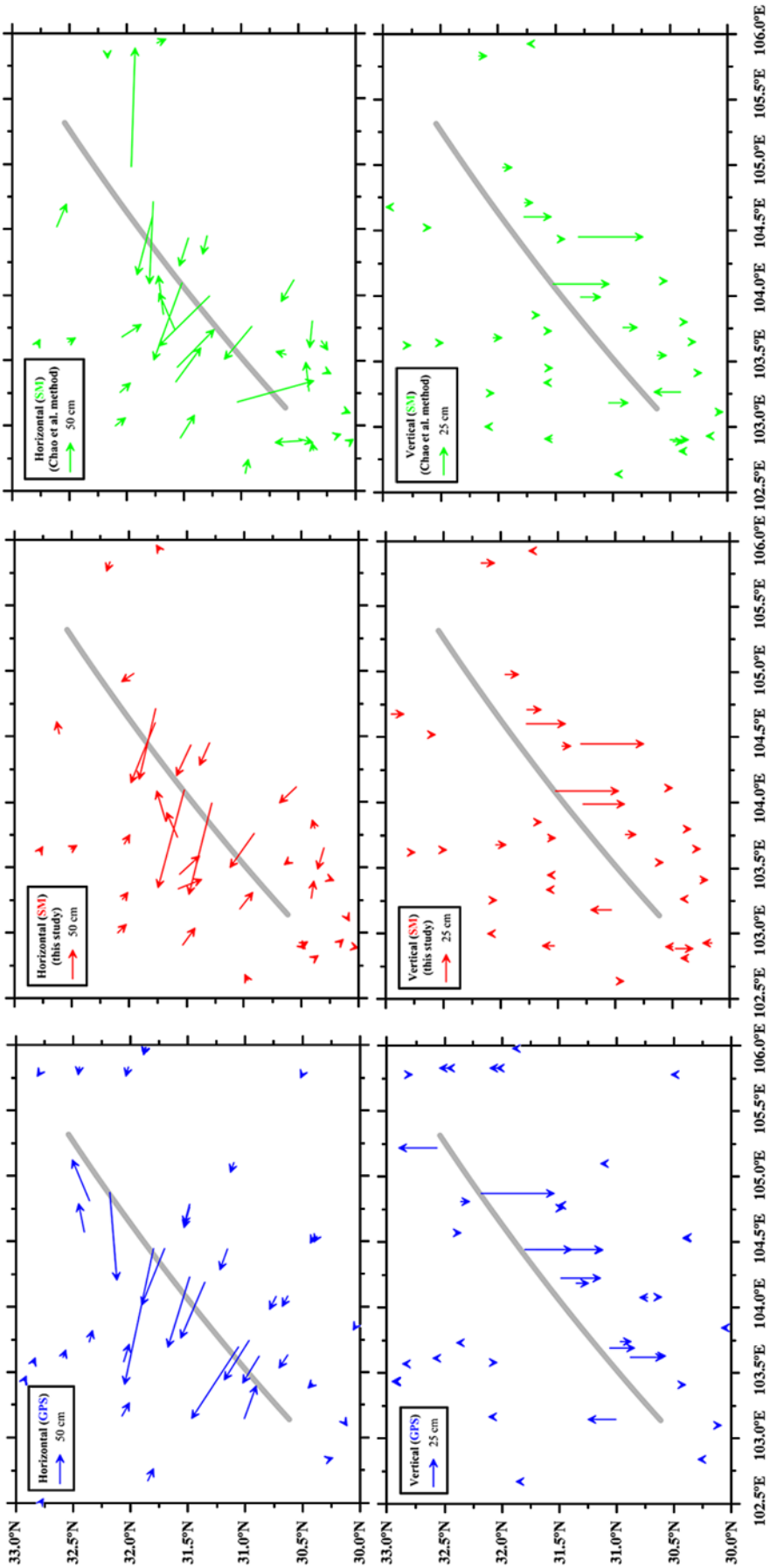

Figure 10. Near-field coseismic displacements of the 2008 M_w 7.9 Wenchuan earthquake determined by the GPS (left) in comparison with that derived from strong-motion records using two different automatic baseline correction schemes (middle and right), respectively. The thick gray line shows a simplified surface trace of the earthquake. The color version of this figure is available only in the electronic edition.

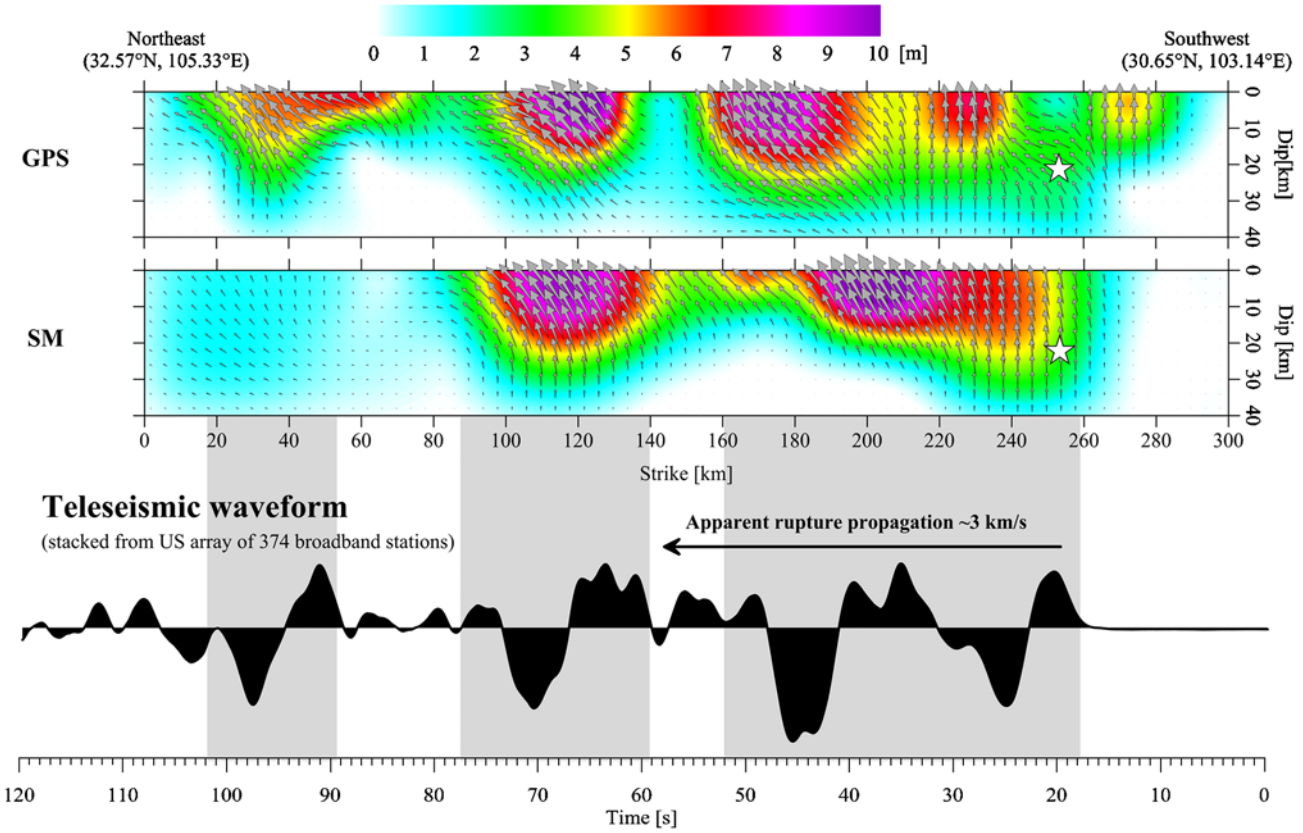

Figure 11. Slip models of the 2008 Wenchuan earthquake derived separately from the GPS and strong-motion (SM) based coseismic static displacement data, compared with a stacked teleseismic waveform from the USArray stations. The assumed fault has a listric geometry with the dip angle linearly decreasing from 60° at the surface to 20° at the bottom. The white star is the hypocenter of the earthquake. The moment magnitudes (M_w) determined by the two slip models are 7.91 (GPS) and 7.87 (SM), respectively. The shadows show the major asperities that can be identified spatially by the slip distribution and temporally by the teleseismic waveform. The color version of this figure is available only in the electronic edition.

magnitude as the displacement seismogram derived from the strong-motion record.

Test Data of a Low-Cost Accelerometer

Recently, an innovative seismic early warning concept, the Self-Organizing Seismic Early Warning Information Network (SOSEWIN), has been developed by the German Research Centre for Geosciences in cooperation with the Humboldt University Berlin (Fleming *et al.*, 2009). Each SOSEWIN node consists of a sensor board and a mini PC. The sensor board is equipped with a low-cost accelerometer (~10 USD as that used in a car airbag system), a GPS time-receiver, and a data processor. So far, no SOSEWIN data have been recorded from the near-field of a large earthquake. We made a laboratory test to investigate whether such a low-cost accelerometer can also be used to recover the low frequency, including static displacement. In this test, a 3D SOSEWIN node was moved by a finite distance on a PVC floor (Fig. 13). The movement was controlled by hand so that it is possibly translational but nonstraight. The data are recorded through three channels: Channel 1 is for the vertical component; Channels 2 and 3 are for the two horizontal components.

As we have done previously, we analyze the test data using our automatic baseline correction scheme blindly. As shown in Figure 14, the results look surprisingly promising. For Channels 1 and 2, the final displacements are recovered almost perfectly. For Channel 3, the recovered displacement is 20% smaller than the true displacement. The Channel 3 component could be recovered better if Boore's $v_f = 0$ option is used, but this is only known with the *a-priori* information. The baseline offsets of the two horizontal components (Channels 2 and 3) appear to be tilt-induced. In contrast, the baseline offset of the vertical component (Channel 1) is untypical, which is caused by the aliasing effect. In fact, the vertical component is of higher frequency that was induced by the roughness of ground and could not be resolved by the 100 Hz digitizer used in the SOSEWIN system.

Discussion and Conclusions

We presented an improved automatic scheme for correcting the event-induced baseline shifts in strong-motion

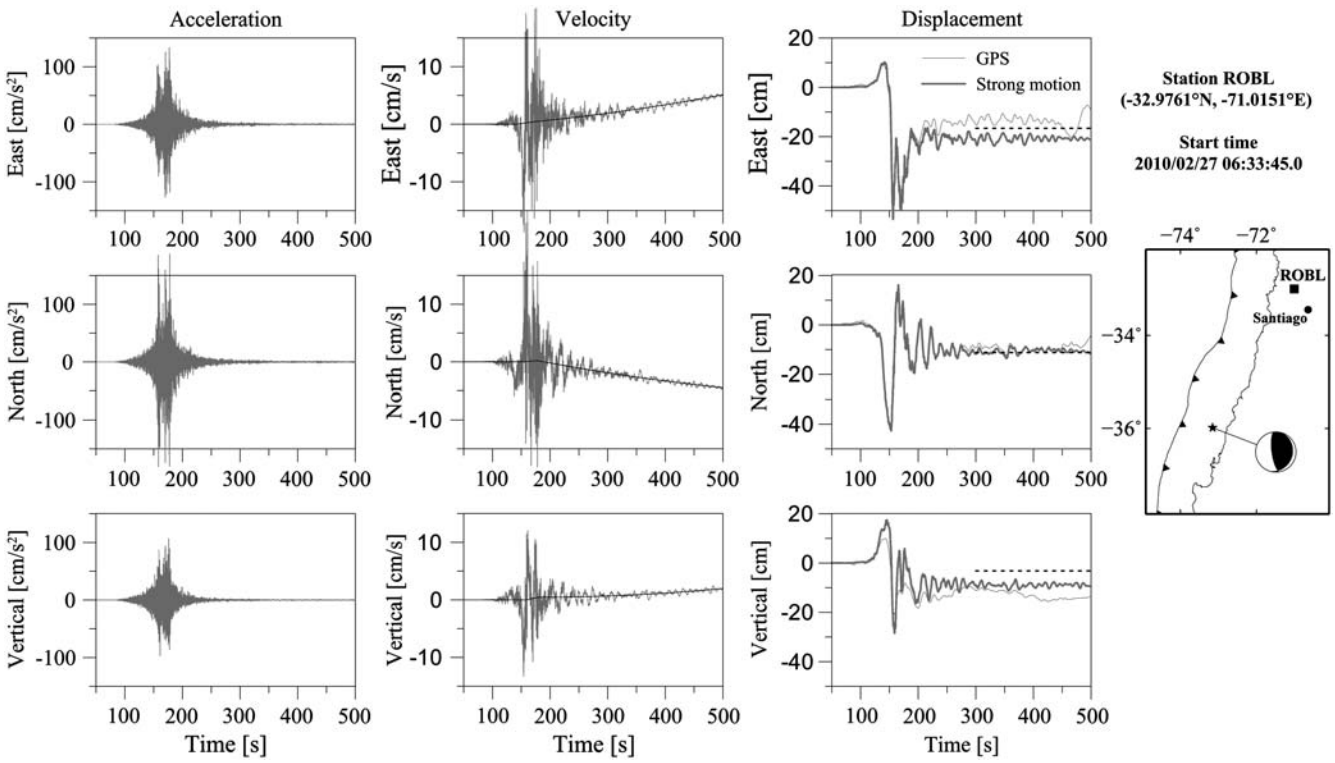

Figure 12. The strong-motion record at station ROBL from the Maule earthquake, the velocity seismograms integrated from the strong-motion records and the trend correction (smooth lines) determined in this study, and the displacement seismograms integrated from the corrected velocity seismograms in comparison with the high-rate (1 Hz) GPS data recorded at the same location. The dotted gray lines show the coseismic displacements (−16.6 cm, −11.2 cm and −3.2 cm) obtained from the daily GPS solutions. The inset map shows the epicenter of the Maule earthquake and station ROBL.

records. In the new scheme, a similar correction form is adopted as suggested by Iwan *et al.* (1985), but no special assumption is made on the sources of the baseline shifts. Instead of a simple threshold approach that is commonly used in previous automatic schemes, a strategy similar to the manually calibrated baseline corrections of Boore (2001) and Wu and Wu (2007), but implemented so no user interference is required, is used to estimate the timing of the baseline shift. First, a most-likely time window of the transient baseline shift is determined by using the velocity and displacement trends as a guide. The optimal timing of the baseline shift is then obtained using a physically reasonable criterion, that is, the corrected displacement history can be approximated by a step function. Moreover, we introduce a technique to minimize the influence of coda waves on the determination of postevent baseline offsets.

The improved automatic scheme is validated by a number of test cases. Several excellent results are achieved under certain optimal condition. Based on our experience, a sufficient but not necessary condition for a successful baseline correction is the single-event characteristic of the strong-motion record at hand. As with the cases shown in Figures 4 and 12, the effective event window is so small that any uncertainty of the transient baseline offset cannot affect the final results dramatically. Notice that the single-event

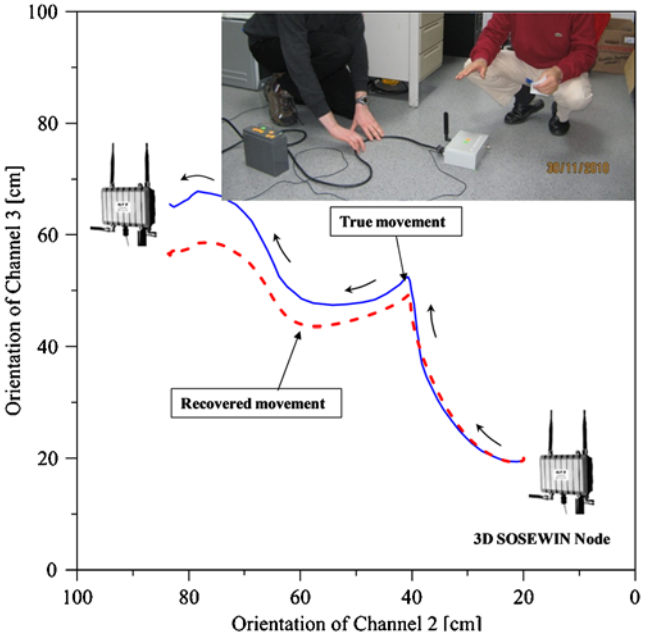

Figure 13. Illustration of the laboratory test of a low-cost accelerometer (3D SOSEWIN node of generation 2). The color version of this figure is available only in the electronic edition.

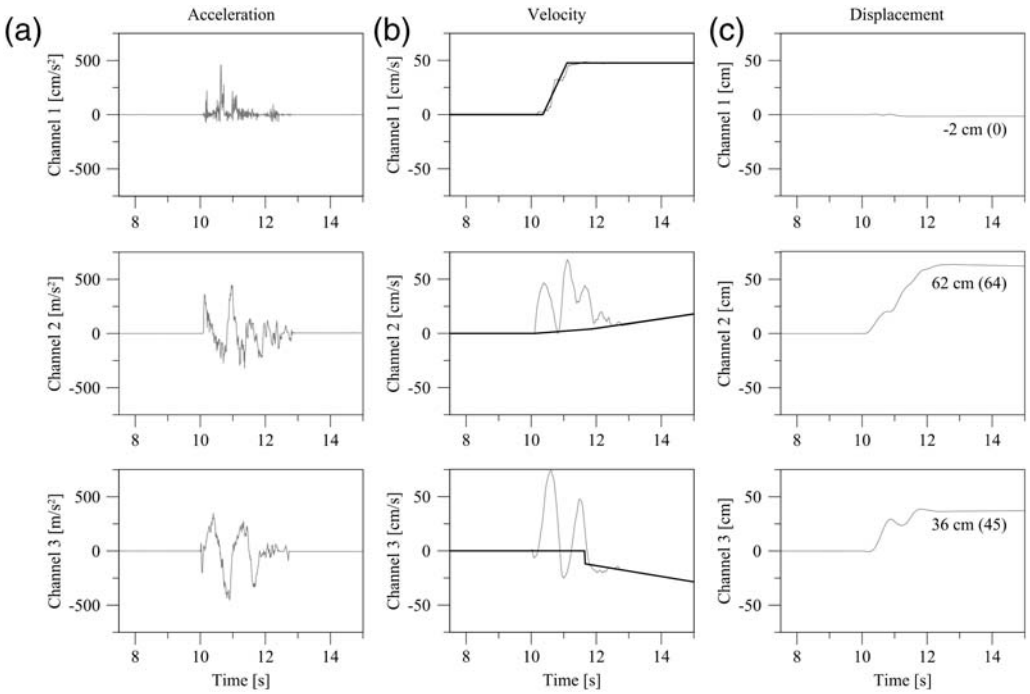

Figure 14. Analysis of the strong-motion record of a 3D SOSEWIN node obtained by the laboratory test shown in Figure 13. (a) Raw data. (b) Velocity time series obtained integrated from the raw data and the trend correction (smooth lines) determined in this study. (c) Displacement time series integrated from the corrected velocity. Channel 1 is the vertical component. Channels 2 and 3 are the two horizontal components. The true values of the final displacements are given by the numbers in the parentheses.

characteristic of a strong-motion record is not necessarily determined by the source process, but mostly by the relative location of observation to the source. At locations close to the source, for example, the strong ground shaking is dominated by the near-field terms of seismic waves that take a short duration and leave a permanent deformation. At locations far from the source, however, the strong ground shaking is dominated by far-field body waves that have no contribution to the static deformation but last long and cause relatively large uncertainties in the empirical baseline correction. In all test cases, the coseismic displacements derived from the strong-motion records agree within about 20% with GPS measurements or model-based predictions. Particularly, the low or null displacements at far-field stations are reproduced robustly, too. An unsolved problem is an objective estimation of uncertainties in the ground acceleration based coseismic displacement data. So far, this can only be done using the *a posteriori* approach if additional geodetic measurements become available. An important conclusion, however, is that if the source area is well covered by strong-motion stations, the magnitude and major slip asperities of the earthquake can be resolved reliably by the ground acceleration based coseismic displacement data. This suggests an implementation of the present baseline correction scheme for the purpose of tsunami early warning and rapid earthquake information systems, particularly in regions where no real-time GPS data are available.

We found that in most cases, the baseline shifts in the two horizontal components are significantly larger than that in the vertical component, indicating that the gravity effect due to ground tilting is a dominant cause. Already a miniscule amount of tilt shows an effect here: for example, the baseline shifts in the strong-motion records at stations TCU052 (Fig. 4) and ROBL (Fig. 12) can be explained by a ground tilt on the order of 0.1° and 0.001°, respectively. For the SOSEWIN test, it is about 0.4° that is realistic for the PVC floor on which the test was made. In comparison, the sources of baseline shift in the vertical component are more complicated. In a few of the test cases, we found that the event-induced baseline offsets in the vertical component are of the same order of magnitude as that in the two horizontal components, which can neither be explained by the gravity effect nor by any rotational ground motion. Thus, unknown instrumental effects might dominate the baseline shifts in the vertical component. It is to be expected that the instrumental effects can be reduced in the future with technical improvements in seismometry. Recently, tests to measure the physically induced baseline shifts using a co-installed three-axis rotational sensor have been conducted (Niggbor, 1994; Graizer, 2005; Lin *et al.*, 2010), but the technique is not yet established. Therefore, the empirical baseline correction approach is still useful before the instrumental problems and the measurement of tilt and rotational motion are solved independently.

Data and Resources

The strong-motion data for the Wenchuan earthquake were provided by China Strong-Motion Networks Centre. The strong-motion and GPS data for the Maule earthquake were provided by Christophe Vigny. The Integrated Plate boundary Observatory in Chile was accessed through the website www.ipoc-network.org (last accessed June 2011). Other data were collected either from the published sources listed in the references or by the authors.

Acknowledgments

We thank Christophe Vigny, Raul Madariaga, Jaime Campos, and Sergio Barrientos for providing the strong-motion and GPS data of the Maule earthquake; the IPOC initiative for the high-quality data from north Chile; Yanlu Ma for preparing the teleseismic data of the Wenchuan earthquake; and Ingo Veigt for supporting the laboratory test. Zhigang Shao is supported by the China Earthquake Administration. Mingpei Jin is supported jointly by the China Scholarship Council and the China Earthquake Administration. In addition, the comments of two anonymous reviewers were very helpful for improving the quality and readability of the paper.

References

Béjar-Pizarro, M., D. Carrizo, A. Socquet, R. Armijo, S. Barrientos, F. Bondoux, S. Bonvalot, J. Campos, D. Comte, J. B. de Chabalier, O. Charade, A. Delorme, G. Gabalda, J. Galetzka, J. Genrich, A. Nercessian, M. Olcay, F. Ortega, I. Ortega, D. Remy, J. C. Ruegg, M. Simons, C. Valderas, and C. Vigny (2010). Asperities and barriers on the seismogenic zone in North Chile: State-of-the-art after the 2007 M_w 7.7 Tocopilla earthquake inferred by GPS and InSAR data, *Geophs. J. Int.* **183,** 390–406.

Boore, D. M. (2001). Effect of baseline corrections on displacement and response spectra for several recordings of the 1999 Chi-Chi, Taiwan, earthquake, *Bull. Seismol. Soc. Am.* **91,** 1199–1211.

Boore, D. M., and J. Bommer (2005). Processing of strong-motion accelerograms: Needs, options and consequences, *Soil Dyn. Earthquake Eng.* **25,** 93–115.

Boore, D. M., C. D. Stephens, and W. B. Joyner (2002). Comments on baseline correction of digital strong-motion data: Examples from the 1999 Hector Mine, California, earthquake, *Bull. Seismol. Soc. Am.* **92,** 1543–1560.

Chao, W., Y. Wu, and L. Zhao (2009). An automatic scheme for baseline correction of strong-motion records in coseismic deformation determination, *J. Seismol.* **14,** 495–504.

Chiu, H. (1997). Stable baseline correction of digital strong-motion data, *Bull. Seismol. Soc. Am.* **87,** 932–944.

Delouis, B., M. Pardo, D. Legrand, and T. Monfret (2009). The M_w 7.7 Tocopilla earthquake of 14 November 2007 at the southern edge of the northern Chile seismic gap: Rupture in the deep part of the coupled plate interface, *Bull. Seismol. Soc. Am.* **99,** 87–94.

Diao, F., X. Xiong, R. Wang, Y. Zheng, and H. Hsu (2010). Slip model of the 2008 M_w 7.9 Wenchuan (China) earthquake derived from the co-seismic GPS data, *Earth Planets Space* **62,** 869–874.

Fleming, K., M. Picozzi, C. Milkereit, F. Kuehnlenz, B. Lichtblau, J. Fischer, C. Zulfikar, O. Ozel, and the SAFER and EDIM working groups (2009). The Self-Organizing Seismic Early Warning Information System (SOSEWIN), *Seismol. Res. Lett.* **80,** 755–771.

Graizer, V. M. (1979). Determination of the true ground displacement by using strong motion records, *Izv. Earth Phys.* **25,** 26–29.

Graizer, V. M. (2005). Effect of tilt on strong motion data processing, *Soil Dyn. Earthq. Eng.* **25,** 197–204.

Graizer, V. (2006). Tilts in strong ground motion, *Bull. Seismol. Soc. Am.* **96,** 2090–2106.

Iwan, W., M. Moser, and C. Peng (1985). Some observations on strong-motion earthquake measurement using a digital acceleration, *Bull. Seismol. Soc. Am.* **75,** 1225–1246.

Klinger, Y., C. Ji, Z. Shen, and W. Bakun (2010). Introduction to the special issue on the 2008 Wenchuan, China, earthquake, *Bull. Seismol. Soc. Am.* **100,** 2353–2356.

Lee, W., T. Shin, K. Kuo, K. Chen, and C. Wu (2001). CWB free-field strong-motion data from the 21 September Chi-Chi, Taiwan, earthquake, *Bull. Seismol. Soc. Am.* **91,** 1370–1376.

Li, X., Z. Zhou, H. Yu, R. Wen, D. Lu, M. Huang, Y. Zhou, and J. Cu (2008). Strong motion observations and recordings from the great Wenchuan earthquake, *Earthquake Eng. Eng. Vib.* **7,** 235–246.

Lin, C. J., H. P. Huang, C. C. Liu, and H. C. Chiu (2010). Application of rotational sensors to correcting rotation-induced effects on accelerometers, *Bull. Seismol. Soc. Am.* **100,** 585–597.

McComb, H. E., A. C. Ruge, and F. Neumann (1943). The determination of true ground motion by integration of strong-motion records: A symposium, *Bull. Seismol. Soc. Am.* **33,** 1–63.

Motagh, M., B. Schurr, J. Anderssohn, B. Cailleau, T. R. Walter, R. Wang, and J.-P. Villotte (2010). Subduction earthquake deformation associated with 14 November 2007, M_w 7.8 Tocopilla earthquake in Chile: Results from InSAR and aftershocks, *Tectonophysics* **490,** 60–68.

Niggbor, R. L. (1994). Six-degree-of-freedom ground-motion measurement, *Bull. Seismol. Soc. Am.* **84,** 1665–1669.

Schurr, B., A. Asch, F. Sodoudi, A. Manzanares, O. Ritter, J. Klotz, G. Chong-Diaz, S. Barrientos, J.-P. Villotte, and O. Oncken (2009). The International Plate Boundary Observatory Chile (IPOC) in northern Chile seismic gap, *Geophys. Res. Abstr.* **11,** Abstract EGU2009-11040.

Segall, P. (2010). *Earthquake and Volcano Deformation*. Princeton University Press, Princeton, New Jersey.

Shen, Z. K., J. Sun, P. Zhang, Y. Wan, M. Wang, R. Bürgmann, Y. Zeng, W. Gan, H. Liao, and Q. Wang (2009). Slip maxima at fault junctions and rupturing of barriers during the 2008 Wenchuan earthquake, *Nat. Geosci.* **2,** 718–724.

Sobolev, S., A. Babeyko, R. Wang, A. Hoechner, R. Galas, M. Rothacher, D. M. Sein, J. Schröter, J. Lauterjung, and C. Subarya (2007). Tsunami early warning using GPS-Shield arrays, *J. Geophys. Res.* **112,** B08415, doi 10.1029/2006JB004640.

Trifunac, M. D. (1971). Zero baseline correction of strong-motion accelerograms, *Bull. Seismol. Soc. Am.* **61,** 1201–1211.

Wang, G., D. M. Boore, H. Igel, and X. Zhou (2003). Some observations on colocated and closely spaced strong ground-motion records of the 1999 Chi-Chi, Taiwan, earthquake, *Bull. Seismol. Soc. Am.* **93,** 674–693.

Wang, G., D. M. Boore, G. Tang, and X. Zhou (2007). Comparisons of ground motions from colocated and closely spaced one-sample-per-second global positioning system and accelerograph recordings of the 2003 M 6.5 San Simeon, California, earthquake in the Parkfield region, *Bull. Seismol. Soc. Am.* **97,** 76–90.

Wang, R., F. Lorenzo-Martín, and F. Roth (2003). Computation of deformation induced by earthquakes in a multi-layered elastic crust—FORTRAN programs EDGRN/EDCMP, *Computer and Geosciences* **29,** 195–207.

Working Group of the Crustal Motion Observation Network of China Project (2008). Coseismic displacement field of the 2008 M_s 8.0 Wenchuan earthquake determined by GPS, *Sci. China Ser. D* **38,** 1195–206 (in Chinese).

Wu, Y., and C. Wu (2007). Approximate recovery of coseismic deformation from Taiwan strong-motion records, *J. Seismol.* **11,** 159–170.

Xu, C., Y. Liu, Y. Wen, and R. Wang (2010). Coseismic slip distribution of the 2008 M_w 7.9 Wenchuan earthquake from joint inversion of GPS and InSAR data, *Bull. Seismol. Soc. Am.* **100,** 2736–2749.

Zhang, P., X. Wen, Z. Shen, and J. Chen (2010). Oblique, high-angle, listric-reverse faulting and associated development of strain: The Wenchuan earthquake of May 12, 2008, Sichuan, China, *Annu. Rev. Earth Planet. Sci.* **38,** 353–382.

Zhu, L. (2003). Recovering permanent displacements from seismic records of the June 9, 1994 Bolivia deep earthquake, *Geophys. Res. Lett.* **30,** 1740.

Helmholz Centre Potsdam
GFZ German Research Centre for Geosciences
Telegrafenberg, D-14473
Potsdam, Germany
wang@gfz-potsdam.de
(R.W., B.S., C.M.)

Institute of Earthquake Science
China Earthquake Administration
Beijing 100049, China
(Z.S.)

Western Yunnan Earthquake Prediction Test Site
China Earthquake Administration
Yunnan Dali 671000, China
(M.J.)

Manuscript received 1 February 2011